Laser Cladding System with Deep Learning Capability

1st Sheng-Yi Tang
Department of Power Mechanical Engineering
National Formosa University
Yunlin, Taiwan
arthurta@nfu.edu.tw

2nd Jie-Ren Shie
Department of Power Mechanical Engineering
National Formosa University
Yunlin, Taiwan
shieji@nfu.edu.tw

3rd Yong-Nong Chang*
Department of Electrical Engineering
National Formosa University
Yunlin, Taiwan
ynchang@gs.nfu.edu.tw

4th Yu-Siang Gu
Department of Power Mechanical Engineering
National Formosa University
Yunlin, Taiwan
johngu0127@gmail.com

***Abstract*—This study establishes a laser cladding system integrated with the YOLOv5 model. This system can identify various cladding conditions, including normal cladding, pore defects, lack of fusion, and overfusion, in production line applications. Its hardware consists of a power supply, a laser cladding module, an optical filter, a camera, and a computer, and its software consists of a software flowchart and the YOLOv5 model. This flowchart enables image acquisition, feature annotation, dataset construction, parameter configuration, and model training and testing. The YOLOv5 model was evaluated using the following parameters: confusion matrix, mean average precision, confidence score, precision, recall, and F1-score. The experimental results confirm that the proposed system achieved high stability and demonstrated strong applicability for real-world defect detection in laser cladding processes.**

***Keywords*—Confidence score, F1-score, laser cladding, software flowchart, YOLOv5**

I. INTRODUCTION

Laser cladding can be used in surface repair and in the reinforcement of mechanical components, molds, turbine blades, and aerospace structures. This technique utilizes a high-power laser beam focused on the workpiece surface to locally melt alloy powders, which, upon cooling, form a high-hardness coating layer. This process offers several advantages, including precise control of the cladding thickness, strong adhesion, and high durability [1]–[3].

During large-scale laser cladding, defects such as cracks, pores, and clad layer delamination are likely to occur. Conventional defect detection methods such as ultrasonic and X-ray inspection often rely on professional interpretation, which introduces subjectivity and poses a risk of misjudgment. Therefore, to improve the quality of clad layers, process parameters such as laser power, scanning speed, powder feed rate, and overlap ratio must be carefully considered. These parameters are typically obtained through repeated experiments. However, identifying effective values and establishing accurate parameter models can be challenging. In addition, traditional laser cladding systems operate in an open-loop manner, which renders the cladding process susceptible to instability due to variations in reflectivity and thermal conductivity and due to environmental disturbances. To enhance quality inspection, optimize process parameters, and increase system stability, deep learning algorithms must be integrated into laser cladding systems to enable the real-time image-based control of cladding layers [4]–[6].

Multiple studies have applied deep learning and machine learning algorithms in the field of machining. In [7], machine learning algorithms combined with a finite element analysis were used to examine the effects of different surface roughness parameters on the fatigue life of TC17 titanium alloy impellers. In that study, a back-propagation artificial neural network was used to predict the influence of surface roughness on fatigue life. In [8], feature fusion and sparse Bayesian learning were used to reduce the milling machining errors of robotic systems and achieve error control for large-scale complex surfaces. In [9], support vector machines were used to classify defects such as pores and lack of fusion, with this followed by the application of Gaussian process regression to predict the effects of process parameters such as laser power, scanning speed, and powder feed rate on pore formation. In [10], a physics-informed machine learning model was proposed that demonstrated simplicity, high efficiency, and high accuracy, with the model enabling the precise prediction of the notch fatigue life of polycrystalline alloys.

In practical laser cladding production, the quality of the clad layer is strongly influenced by process parameters, and inappropriate parameter selection may lead to defects such as pores, a lack of fusion, or overfusion. These defects prevent the clad layer from meeting design requirements, and they increase the risk of product failure (Fig. 1). Pores are small voids or bubbles that form in the bonding region between the clad layer and the substrate. These pores are typically caused by gas entrapment, incomplete molten pool solidification, or insufficient metallurgical bonding between materials. A lack of fusion indicates the presence of gaps or weakly bonded regions between the clad layer and the substrate, and this can create structural weak points. Overfusion occurs when the laser output power is excessively high during cladding. It results in an overly deep molten pool that compromises the microstructure and performance of the clad layer.

This study developed a laser cladding system integrated with a software flowchart and the YOLOv5 model to identify and classify defects and to construct a defect database. Experimental validation of this system revealed it to achieve high performance in defect recognition and classification.

The remainder of this paper is organized as follows. Section II describes the operating principle of the proposed laser cladding system along with its software flowchart. Section III presents the experimental results and their analysis. Section IV concludes the study.

Fig. 2 illustrates the composition of the power supply and the laser cladding system. The power supply consists of an AC power source, a power factor correction (PFC) circuit, and a DC–DC converter. Its operating principle is that AC input passes through the PFC circuit to align the phase of the input voltage and current and improve the power factor. Subsequently, the DC–DC converter transforms high-voltage DC into low-voltage DC to feed the laser device. The laser cladding system consists of a laser unit, a powder feeder, an optical filter, a camera, and a computer. Its operating principle is that the interaction between the laser beam and the powder feed generates a melt pool on the workpiece. During this process, images of the molten pool are captured by the camera through the optical filter, compiled into a database, and analyzed as outlined in Fig. 3. After execution of the software flowchart, a feedback signal, denoted as $Sig_{Feedback}$, is generated and transmitted to the DC–DC converter. $Sig_{Feedback}$ is compared with the internal triangular carrier signal of the converter to generate the corresponding pulse-width modulation (PWM) signal. By modulating the PWM signal, the input voltage of the laser cladding system is regulated, thereby enabling adjustment of the laser output power.

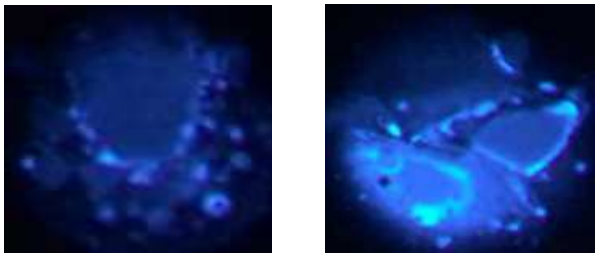

(a) Pore (b) Lack of fusion

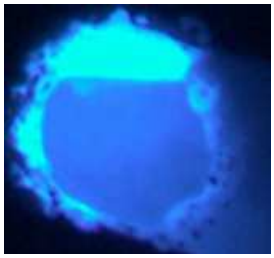

(c) Overfusion

Fig. 1. Defect types in laser cladding.

II. Laser Cladding System

Fig. 3 presents the proposed software workflow, which is divided into two components: a labeled database on the left and the YOLOv5 model on the right. As indicated on the left of the figure, images are captured by the camera until a clear frame is obtained. Each image is then processed in Roboflow to a resolution of 640 × 640 × 3 pixels, and data augmentation is applied to expand the dataset size by a factor of three. Subsequently, bounding boxes are applied to annotate the images into four categories: normal cladding, pore defects, lack of fusion, and overfusion. These annotated images are then compiled into training and testing datasets for the YOLOv5 model. As indicated on the right of Fig. 3, training is conducted using train.py with the following parameters: batch size = 16, initial learning rate = 0.001, epochs = 300, confidence score threshold = 0.25, maximum number of detection operations = 1000, and regional threshold = 1000 px^2. An early stopping mechanism is employed to prevent overfitting and terminate the training process when the relative variation in validation loss remains below 1 for 20 consecutive epochs. Finally, the YOLOv5 model is trained and tested using the constructed datasets, and its performance is evaluated in terms of stability, confusion matrix, mean average precision (mAP), confidence score, precision, recall, and F1-score.

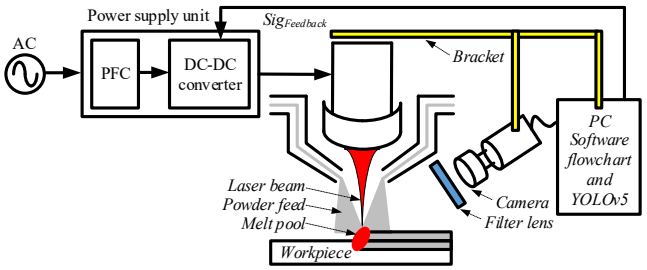

Fig. 2. Laser cladding system.

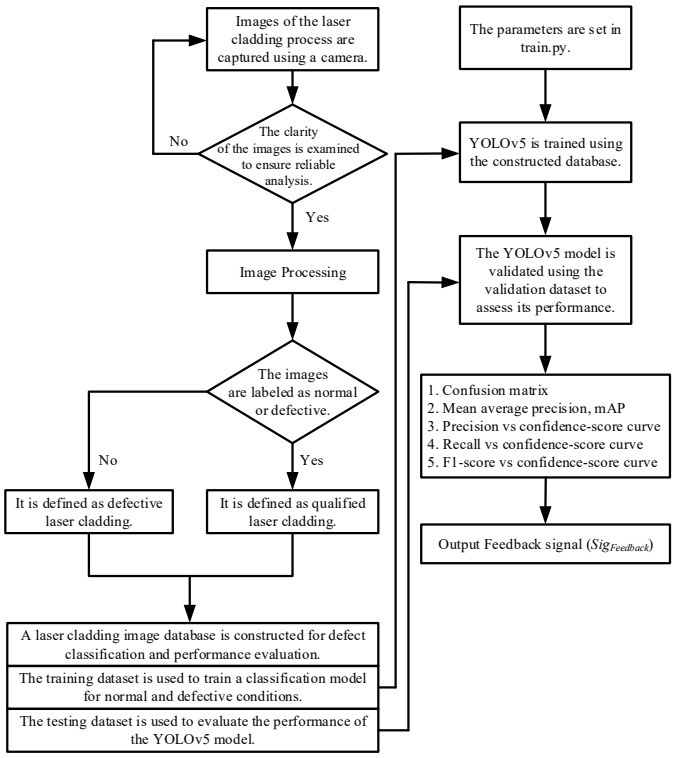

Fig. 3. Software flowchart

III. Experimental Results and Analysis

Fig. 4 depicts the confusion matrix, which demonstrates the correspondence between the actual annotations and model predictions, with this used to further evaluate the ability of the YOLOv5 model to identify normal and defect phenomena during laser cladding. In Fig. 4, the horizontal axis represents the ground-truth labels, whereas the vertical axis represents the predicted labels. Each numerical value corresponds to a normalized proportion, with darker colors indicating higher ratios. As presented in Fig. 4, the classification accuracy for lack of fusion, normal cladding, overfusion, and pore defects is 100%, 94%, 87%, and 91%, respectively. The background false positive rate (FP2) for lack of fusion and overfusion is only 20%, indicating the model has high recognition capability for these two types of defects. However, the false positive rate for normal cladding is 60%, indicating that under specific conditions, the model may fail to accurately identify the cladding region. In practical production lines, such conditions may lead to reduced yield, which may in turn affect the stability and automation benefits of laser cladding systems.

To address the aforementioned problems, this paper presents an analysis of the problems from four perspectives: a human perspective, a machine perspective, a material perspective, and a methodological perspective.

1. Human perspective: Nonuniform annotations of normal laser cladding samples cause learning bias in the model, whereas a lack of classification knowledge among annotators results in labeling discrepancies.

2. Machine perspective: The imaging process of the camera is influenced by environmental and lighting disturbances, leading to nonuniform image quality and reduced recognition accuracy.
3. Material perspective: The surface roughness and reflectivity of materials introduce errors in mask segmentation, which in turn affects the model's ability to accurately identify cladding regions.
4. Methodological perspective: Inappropriate settings for training parameters (e.g., anchor, boxes, and learning rate) may cause deviations during the training process.

Future studies can enhance the recognition accuracy of the YOLOv5 model for laser cladding systems by addressing these four problems.

Fig. 5 presents the mAP results. "Box" evaluation involves an analysis of whether the bounding box drawn by the model successfully "captures" the defect, which is a coarse-level detection criterion focusing on "hit or miss." "Mask" evaluation refers to the measurement of the pixel-wise overlap between the predicted mask and the ground-truth defect contour, and it reflects segmentation accuracy, which provides a fine-grained assessment of detection quality. At an intersection over union (IoU) of 0.5—as depicted in Fig. 5(a), "Box" evaluation revealed an mAP of 0.992, and—as depicted in Fig. 5(b)—"Mask" evaluation revealed an mAP of 0.987. These results indicate that at a relaxed overlap threshold, all samples can be completely detected and correctly classified. At an IoU of 0.5–0.95 (step = 0.05)—as depicted in Fig. 5(c), "Box" evaluation revealed an mAP of 0.868, and—as depicted in Fig. 5(d)—"Mask" evaluation revealed an mAP of 0.838. These results indicate that under stricter conditions, the YOLOv5 model still achieves a mean precision of approximately 87% and 84% for defect bounding box localization and mask-based segmentation, respectively.

Fig. 6 illustrates the precision versus confidence score curves of the YOLOv5 model for normal cladding and the three types of defects. These curves demonstrate the relationship between prediction confidence scores and precision at varying decision thresholds and served as a key reference for selecting an appropriate confidence score threshold in this study. In Fig. 6, the horizontal axis represents the confidence scores assigned by the model to its predictions, whereas the vertical axis represents the corresponding precision values. Four observations can be made from the figure:

1. When the confidence score increases, the precision of all curves demonstrates an upward trend, indicating that precision is positively correlated with confidence score.
2. Compared with other categories, NG_1 (lack of fusion) and NG_2 (overfusion) exhibit more stable performance, with smooth curves that rapidly reach high precision, indicating the model is effective in identifying these types of defects with distinct characteristics.
3. Compared with other categories, NG_3 (pores) achieves slightly lower precision but still approaches 0.95. This low performance is attributable to the irregular shapes and relatively small areas of pores, which pose major challenges for the model.
4. When normal cladding occurs, when the confidence score reaches 0.02, the degree of precision remains above 0.8 and continues to increase. This result indicates that the model rarely misclassifies normal regions as defects, which is useful in reducing false positive rates.

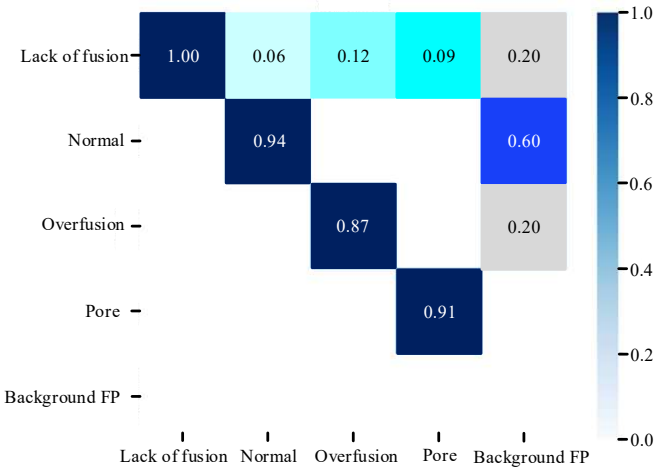

Fig. 4. Confusion matrix

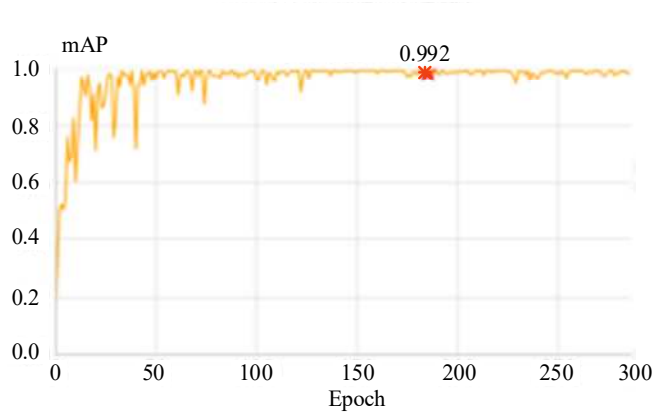

(a) IoU = 0.5, Box mode

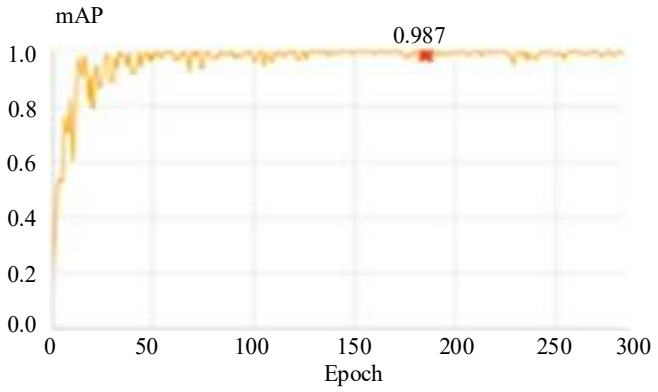

(b) IoU = 0.5, Mask mode

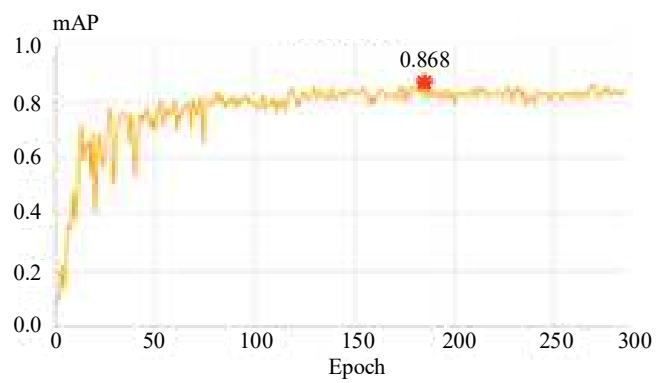

(c) IoU = 0.5–0.95, Box mode

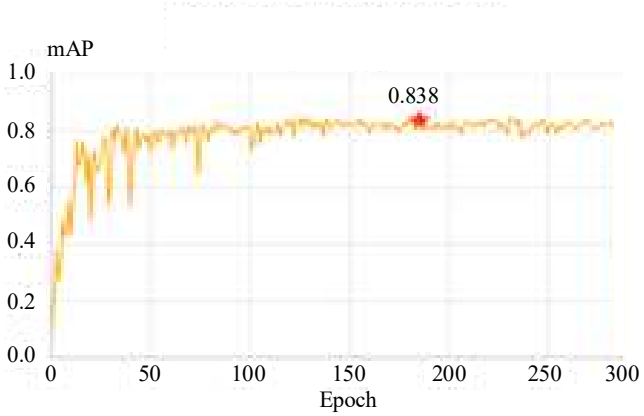

(d) IoU = 0.5–0.95, Mask mode

Fig. 5. mAP results.

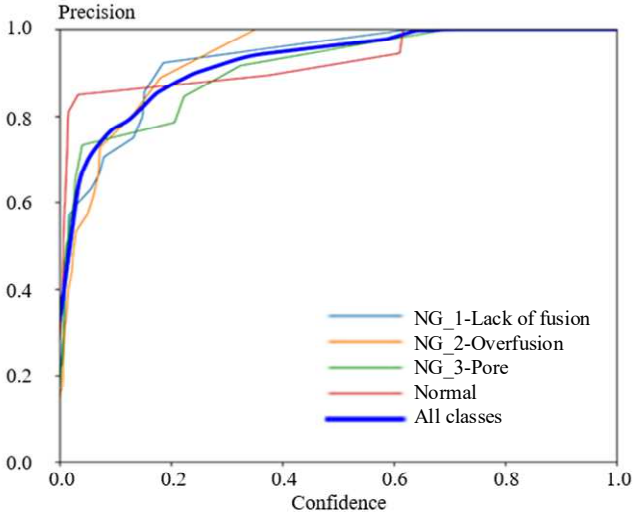

Fig. 6. Precision versus confidence score curves.

Fig. 7 illustrates the recall versus confidence score curves of the YOLOv5 model for normal cladding and the three types of defects. These curves demonstrate the proportion of actual defects that can be detected. In Fig. 7, the horizontal axis represents the confidence scores assigned by the model to its predictions, whereas the vertical axis represents the corresponding recall rates. Four observations can be made from the figure:

1. When the confidence score approaches zero, the recall rate reaches 1.00 across all categories. This result suggests that with a relaxed prediction threshold, the model can cover all ground-truth samples, indicating it has strong detection capability.
2. When the confidence score increases, the recall rate rapidly decreases, indicating that with a strict prediction threshold, the model achieves high precision but low recall, which leads to missed detection.
3. For category NG_3 (pores), the recall rate even remains high when the confidence score exceeds 0.7, suggesting the model is able to identify subtle defect features.
4. For categories NG_1 (lack of fusion) and NG_2 (overfusion), when the confidence score is 0.7, the recall rate remains above 0.8 across all categories, indicating the model is able to detect unfused and overmelted defects. However, when the confidence score exceeds 0.7, the recall rate rapidly decreases, leading to frequent missed detection. This phenomenon indicates a need for further optimization in subsequent studies.

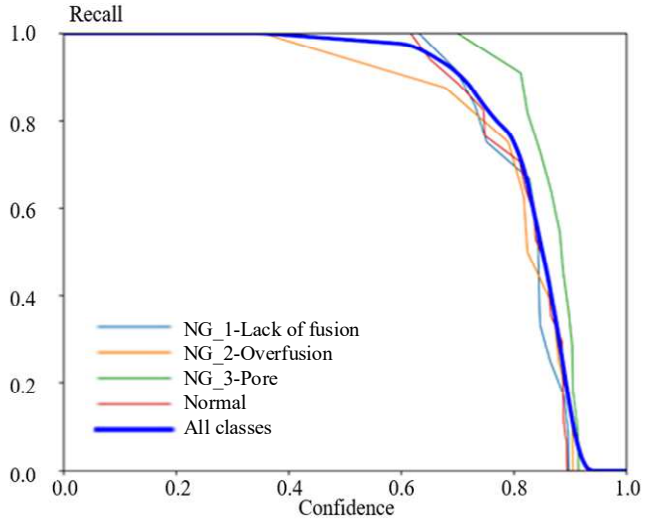

Fig. 7. Recall versus confidence score curves.

Fig. 8 illustrates the F1-score versus confidence score curves of the YOLOv5 model for normal cladding and the three types of defects. In this figure, the F1-score represents the harmonic mean of precision and recall. In addition, the horizontal axis represents the prediction confidence scores, whereas the vertical axis represents the F1-scores. Three observations can be made from the figure:

1. When the confidence score ranges from 0.3 to 0.7, the F1-scores of all categories remain at approximately 0.9, indicating that the model maintains its performance within this interval. This range is therefore suitable as a reference threshold for practical applications.
2. When the confidence score ranges from 0.22 to 0.82, category NG_3 (pores) achieves the highest performance, consistently maintaining a high F1-score of approximately 0.9. This finding suggests that pore defects exhibit distinct characteristics that can be effectively recognized by the model.
3. When the confidence score ranges from 0.3 to 0.7, the F1-scores of all categories reach approximately 0.92, indicating nearly optimal precision and recall. This finding confirms the appropriateness of the image labeling strategy and the training methodology utilized by the model.

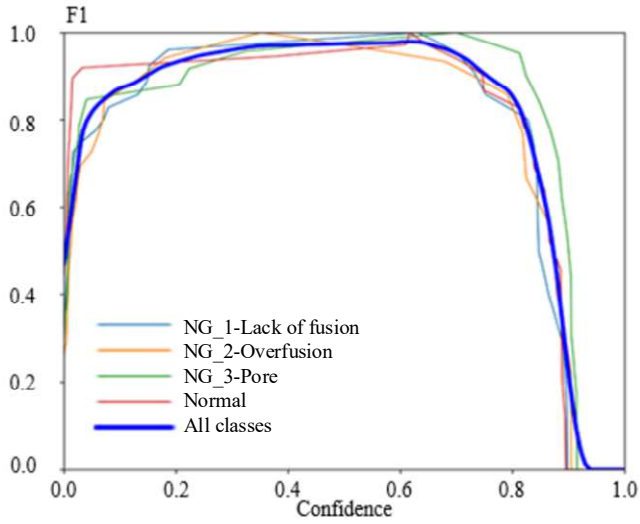

Fig. 8. F1-score versus confidence score curves.

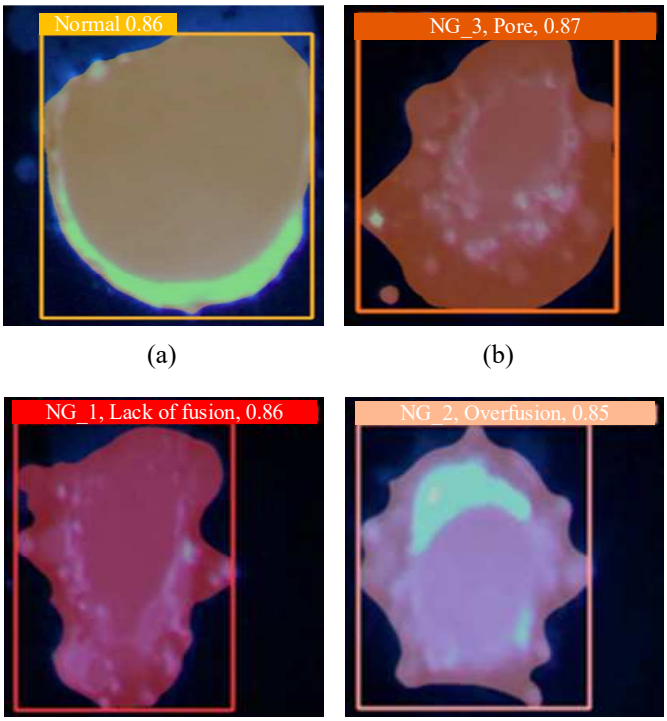

Fig. 9. Detection results of the YOLOv5 model.

In this study, a YOLOv5 model was developed to classify normal and defect phenomena in laser cladding. The model's performance was validated on an automated production line. As presented in Fig. 9, the proposed model identified (a) normal cladding with a confidence score of 0.86, (b) a pore defect with a confidence score of 0.87, (c) a lack-of-fusion defect with a confidence score of 0.86, and (d) an overfusion defect with a confidence score of 0.85. These experimental results confirm the model's high feasibility for practical applications.

IV. Conclusion

This paper presents a novel laser cladding system integrated with the YOLOv5 model. This system is capable of identifying different cladding conditions, including normal cladding, pore defects, a lack of fusion, and overfusion. For the curves of precision versus confidence score, when the confidence score threshold is 0.2, the recognition accuracy of all categories remains above 0.8, with lack of fusion and overfusion exhibiting the highest performance. For the curves of recall versus confidence score, when the confidence score threshold is 0.7, the recall rate of all categories remains above 0.8, although the risk of missed detection increases at this threshold. For the curves of F1-score versus confidence score, when the confidence score ranges between 0.3 and 0.7, the F1-scores of all categories approach 0.92, indicating nearly optimal precision and recall. According to the results of small-scale production tests, the confidence scores of all categories fall within the range of 0.85 to 0.87, confirming the proposed system's high stability and strong feasibility. Future studies should focus on validating the proposed system within large-scale production environments.

References

[1] C. Y. Zhu, H. Zhu and S. J. Zhone, "Laser cladding path planning algorithm based on surface point cloud data," in *proc. IEEE 7th International Conference on Data Science and Information Technology*, Dec. 2024, pp. 1–6.

[2] H. Zhu and S. Wang, "3D reconstruction and path planning of complex parts for laser cladding," in *proc. IEEE 9th International Conference on Image*, Vision and Computing, July. 2024, pp. 1–6.

[3] M. Liu, Y. Cai, C. Duan, and G. Li, "Key techniques in parts repair and remanufacturing based on laser cladding: A review," *Journal of Manufacturing Processes*, vol. 132, pp. 994-1014, Dec. 2024.

[4] Z. Liu and C. Liu, "Deep learning-assisted numerical simulation of laser cladding for cold-rolled rolls," in *proc. IEEE Congress on Evolutionary Computation, June*. 2025, pp. 1–4.

[5] S. J. Zhong, H. Zhu and C. Y. Zhu, "Optimisation of continuous overlapping point cloud data for laser cladding," in *proc. IEEE 7th International Conference on Data Science and Information Technology*, Dec. 2024, pp. 1–5.

[6] X. C. Ji, R. S. Chen, C.X. Lu, J. Zhou, M. Q. Zhang, T. Zhang, H. L. Yu, Y. L. Yin, P. J. Shi and W. Zhang, "Recent advances in machine learning for defects detection and prediction in laser cladding process," *Journal of Next Materials*, vol. 7, pp. 1-21, April 2024.

[7] W. Jinlong, M. Yuxin, P. Wenjie, B. Yongjie and S. Zeyu, "Evaluation of the effect of surface roughness parameters on fatigue of TC17 titanium alloy impeller using machine learning algorithm and finite element analysis," *Journal of Engineering Failure Analysis*, vol. 153, pp. 1-15, Nov. 2024.

[8] S. Zhao, H. Sun, F. Peng, R. Yan, X. Tang, Y. Shan and J. Su, "Feature fusion and distillation embedded sparse Bayesian learning model for in-situ foreknowledge of robotic machining errors," *Journal of Journal of Manufacturing Systems*, vol. 71, pp. 546-564, Dec. 2023.

[9] J. A. Lee, M. J. Sagong, J. Jung, E. S. Kim and H. S. Kim, "Explainable machine learning for understanding and predicting geometry and defect types in Fe-Ni alloys fabricated by laser metal deposition additive manufacturing," *Journal of Materials Research and Technology*, vol. 22, pp. 413-423, Jan.-Feb. 2023.

[10] W. Q. Hao, L. Tan, X. G. Yang, D. Q. Shi, M.L. Wang, G. L. Miao and Y.S. Fan, "A physics-informed machine learning approach for notch fatigue evaluation of alloys used in aerospace," *International Journal of Fatigue*, vol. 170, pp. 1-15, May 2023.